Atmos. Chem. Phys. Discuss., https://doi.org/10.5194/acp-2017-904
Manuscript under review for journal Atmos. Chem. Phys.
Discussion started: 23 November 2017

Atmospheric Chemistry and Physics
Discussions

Decrease in tropospheric O_3 levels of the Northern Hemisphere observed by IASI

Catherine Wespes[1], Daniel Hurtmans[1], Cathy Clerbaux[1,2], Anne Boynard[2] and Pierre-François Coheur[1]

[1]Spectroscopie de l'Atmosphère, Service de Chimie Quantique et Photophysique, Faculté des Sciences, Université Libre de Bruxelles (ULB), Bruxelles, Belgique
[2] LATMOS/IPSL, UPMC Univ. Paris 06 Sorbonne Universités, UVSQ, CNRS, Paris, France

Abstract

In this study, we describe the recent changes in the tropospheric ozone (O_3) columns (TOCs) measured by the Infrared Atmospheric Sounding Interferometer (IASI) onboard the Metop satellite during the first 9 years of the IASI operation (January 2008 to May 2017). Using appropriate multivariate regression methods, we discriminate significant linear trends from other sources of O_3 variations captured by IASI. The geographical patterns of the adjusted O_3 trends are provided and discussed on the global scale. Given the large contribution of the natural variability in comparison with that of the trend (25-85% *vs* 15- 50%, respectively) to the total O_3 variations, we estimate that additional years of IASI measurements are generally required to detect the estimated O_3 trends with a high precision. Globally, additional 6 months to 6 years of measurements, depending on the regions and the seasons, are needed to detect a trend of |5| DU/decade. An exception is interestingly found during summer in the mid-high latitudes of the North Hemisphere (N.H.; ~ 40°N-75°N) where the large absolute fitted trend values (~|0.5| DU/yr on average) combined with the small model residuals (~10%) allow the detection of a band-like pattern of significant negative trends. This finding supports the reported decrease in O_3 precursor emissions in recent years, especially in Europe and US. The influence of continental pollution on that latitudinal band is further investigated and supported by the analysis of the O_3-CO relationship (in terms of correlation coefficient, regression slope and covariance) that we found to be the strongest at the northern mid-latitudes in summer.

1 Introduction

O_3 plays a key role throughout the whole troposphere where it is produced by the photochemical oxidation of carbon monoxide (CO), non-methane volatile organic compounds (NMVOCs) and methane (CH_4) in the presence of nitrogen oxides (NO_x) (e.g. Logan et al., 1981). O_3 sources in the troposphere are the in situ photochemical production from anthropogenic and natural precursors, and the downwards transport of stratospheric O_3. Being a strong pollutant, a major reactive species and an important greenhouse gas in the upper troposphere, O_3 is of highest interest for air quality, atmospheric chemistry and radiative forcing studies. Thanks to its long lifetime (several weeks) relatively to transport timescales in the free troposphere (Fusco and Logan, 2003),

Atmos. Chem. Phys. Discuss., https://doi.org/10.5194/acp-2017-904
Manuscript under review for journal Atmos. Chem. Phys.
Discussion started: 23 November 2017

O_3 also contributes to large-scale transport of pollution far from source regions with further impacts on global air quality (e.g. Stohl et al., 2002; Parrish et al., 2012) and climate. Monitoring and understanding the time evolution of tropospheric O_3 at a global scale is, therefore, crucial to apprehend future climate changes. Nevertheless, a series of limitations make O_3 trends particularly challenging to retrieve and to interpret.

Since the 1980s, while the O_3 precursors anthropogenic emissions have increased and shifted equatorward in the developing countries (Zhang et al., 2016), extensive campaigns and routine in situ and remote measurements at specific urban and rural sites have provided long-term but sparse datasets of tropospheric O_3 (e.g. Cooper et al., 2014 and references therein). Ultraviolet and Visible (UV/VIS) atmospheric sounders onboard satellites provide tropospheric O_3 measurements with a much wider coverage, but they result either from indirect methods (e.g. Fishman et al., 2005) or from direct retrievals which are limited by coarse vertical resolution (Liu et al., 2010). All these datasets also suffer from a lack of homogeneity in terms of measurement methods (instrument and algorithm) and spatio-temporal samplings (e.g. Doughty et al., 2011). Those limitations, in addition to the large natural inter-annual variability (IAV) and decadal variations in tropospheric O_3 levels (due to large-scale dynamical modes of O_3 variations and to changes in stratospheric O_3, in stratosphere-troposphere exchanges, in precursor emissions and in their geographical patterns), introduce strong biases in trends determined from independent studies and datasets (e.g. Zbinden et al., 2006; Thouret et al., 2006; Logan et al., 2012 ; Parrish et al., 2012 and references therein). As a consequence, determining accurate trends requires a long period of high density and homogeneous measurements (e.g. Payne et al., 2017).

Such long-term datasets are now becoming obtainable with the new generation of nadir-looking and polar-orbiting instruments measuring in the thermal infrared region. In particular, about one decade of O_3 profile measurements, with a good sensitivity in the troposphere independently from the layers above, is now available from the IASI (Infrared Atmospheric Sounding Interferometer) sounder aboard the European Metop platforms, allowing to monitor regional and global variations in tropospheric O_3 levels (e.g. Dufour et al., 2012; Safieddine et al., 2013; Wespes et al., 2016).

In this study, we examine the tropospheric O_3 changes behind the natural IAV as measured by IASI over January 2008-May 2017. To that end, we use the approach described in Wespes et al. (2017), which relies on a multi-linear regression (MLR) procedure, for accurately differentiating trends from other sources of O_3 variations; the latter being robustly identified and quantified in that companion study. In Section 2, we briefly review the IASI mission and the tropospheric O_3 product, and we shortly describe the multivariate models (annual or seasonal) that we use for fitting the daily O_3 time series. In Section 3, after verifying the performance of the MLR models over the available IASI dataset, we evaluate the feasibility to capture and retrieve significant trend characteristics, apart from natural O_3 dependencies, by performing trend sensitivity studies. In Section 4, we present and discuss the global distributions of the O_3 trends estimated from IASI in the troposphere. The focus is given in summer over and downwind anthropogenic polluted areas of the N.H. where the possibility to infer significant trends from the first ~9 years of available IASI measurements is demonstrated. Finally, the O_3-CO correlations, enhancement ratios and covariance are examined for characterizing the origin of the air masses in regions of positive and negative trends.

2 IASI O_3 measurements and multivariate regression

The IASI instrument is a nadir-viewing Fourier transform spectrometer that records the thermal infrared emission of the Earth-atmosphere system between 645 and 2760 cm^{-1} from the polar Sun-synchronous orbiting meteorological Metop series of satellites. Metop-A and –B have been successively launched in October 2006 and September 2012. The third and last launch is planned in 2018 with Metop-C to ensure homogeneous long-term IASI measurements. The measurements are taken every 50 km along the track of the satellite at nadir and over a swath of 2200 km across track, with a field of view of four simultaneous footprints of 12 km at nadir, which provides global coverage of the Earth twice a day (at 9:30 AM and PM mean local solar time). The instrument presents a good spectral resolution and a low radiometric noise, which allows the retrieval of numerous gas-phase species in the troposphere (e.g. Clerbaux et al., 2009, and references therein; Hilton et al., 2012; Clarisse et al., 2011).

In this paper, we use the FORLI-O_3 profiles (Fast Optimal Retrievals on Layers for IASI processing chain set up at ULB; v20151001) retrieved from the IASI-A (aboard Metop-A) daytime measurements (defined with a solar zenith angle to the sun < 80°) which result from a good spectral fit (determined here by quality flags on biased or sloped residuals, suspect averaging kernels, maximum number of iteration exceeded,…). These profiles are characterized by a good vertical sensitivity to the troposphere and the stratosphere (e.g. Wespes et al., 2017). The FORLI algorithm relies on a fast radiative transfer and retrieval methodology based on the Optimal Estimation Method (Rodgers, 2000) and is fully described in Hurtmans et al. (2012). The FORLI-O_3 profiles, which are retrieved on 40 constant vertical layers from surface up to 40 km and an additional 40-60 km one, have already undergone thorough characterization and validation exercises (e.g. Anton et al., 2011; Dufour et al., 2012; Gazeaux et al., 2012; Hurtmans et al., 2012; Parrington et al., 2012; Pommier et al., 2012; Scannell et al., 2012; Oetjen et al., 2014; Boynard et al., 2016; Wespes et al., 2016; Keppens et al. 2017; Boynard et al., 2017). They demonstrated a good degree of accuracy, of precision and of vertical sensitivity with no drift, to capture the large-scale dynamical modes of O_3 variability in the troposphere independently from the layers above (Wespes et al., 2017), with the possibility to further differentiate long-term O_3 changes in the troposphere (Wespes et al., 2016).

For this purpose, we focus, in this work, on a tropospheric column ranging from ground to 300 hPa that includes the altitude of maximum sensitivity of IASI in the troposphere (usually between 4

Atmos. Chem. Phys. Discuss., https://doi.org/10.5194/acp-2017-904
Manuscript under review for journal Atmos. Chem. Phys.
Discussion started: 23 November 2017

Atmospheric Chemistry and Physics
Discussions

and 8 km altitude), limits as much as possible the influences of the stratospheric O_3 and that was shown in Wespes et al. (2017) to exhibit independent deseasonalized anomalies/dynamical processes from those in the stratospheric layers. The stratospheric contribution into the tropospheric O_3 columns have been previously estimated in Wespes et al. (2016) as ranging between 30% and 65% depending on the region and the season with the smallest contribution as well as the largest sensitivity in the northern mid-latitudes in spring-summer where the O_3 variations, hence, mainly originate from the troposphere. We use the same MLR model (in its annual or its seasonal formulation) as the one developed in the companion paper (see Eq.1 and 2; Section 2.2 in Wespes et al., 2017), which includes a series of geophysical variables in addition to a linear trend (LT) term. The MLR which is performed using an iterative stepwise backward elimination approach to retain the most relevant explanatory variables (called “proxies”) at the end of the iterations (e.g. Mäder et al., 2007) is applied on the daily IASI O_3 time series. The main selected proxies used to account for the natural variations in O_3 are namely the QBO (Quasi-Biennial Oscillation), the NAO (North Atlantic Oscillation) and the ENSO (El Niño–Southern Oscillation) (cfr Table 1 in Wespes et al. (2017) for the exhaustive list of the used proxies). Their associated standard errors are estimated from the covariance matrix of the regression coefficients and are corrected to take into account the uncertainty due to the autocorrelation of the noise residual (see Eq. 3 in Wespes et al. (2016)). The common rule that the regression coefficients are significant if they are greater in magnitude than 2 times their standard errors is applied (95% confidence limits defined by 2σ level). The MLR model was found to give a good representation of the IASI O_3 records in the troposphere over 2008-2016, allowing us to identify/quantify the main O_3 drivers with marked regional differences in the regression coefficients. Time-lags of 2 and 4 months for ENSO are also included hereafter in the MLR model to account for a large but delayed impact of ENSO on mid- and high latitudes O_3 variations far from the Equatorial Pacific where the ENSO signal originates (Wespes et al., 2017).

3 Regression performance and sensitivity to trend

In this section, we first verify the performance of the MLR models (annual and seasonal; in terms of residual errors and variation explained by the model) to globally reproduce the time evolution of O_3 records over the entire studied period (January 2008 – May 2017). Based on this, we then investigate the statistical relevance for a trend study from IASI in the troposphere by examining the sensitivity of the pair IASI-MLR to the retrieved LT term.

Figure 1 presents the seasonal distributions of tropospheric O_3 measured by IASI averaged over January 2008 – May 2017 (left panels), along with the root-mean-squared error of the seasonal regression fit (*RMSE*, in DU; middle panels) and the contribution of the fitted seasonal model into the IASI O_3 time series (in %; right panels), calculated as $\frac{\sigma\left(O_3^{\text{Fitted\_model}}(t)\right)}{\sigma\left(O_3(t)\right)}$ where σ is the standard

Atmos. Chem. Phys. Discuss., https://doi.org/10.5194/acp-2017-904
Manuscript under review for journal Atmos. Chem. Phys.
Discussion started: 23 November 2017

deviation relative to the regression models and to the IASI O_3 time series. These two statistical parameters help to evaluate how well the fitted model explains the variability in the IASI O_3 observations. The seasonal patterns of O_3 measurements are close to those reported in Wespes et al. (2017) for a shorter period (see Section 2.1 and 3.1 in Wespes et al. (2017) for a detailed description of the distributions) and they clearly show, for instance, high O_3 values over the highly populated areas of Asia in summer. The distributions from Fig.1 show that the model reproduces between 35% and 90% of the daily O_3 variation captured by IASI and that the residual errors varies between 0.01 DU and 5 DU (i.e. the *RMSE* relative to the IASI O_3 time series are of ~15% on global average and vary between 10% in the N.H. in summer and 30% in specific tropical regions). On an annual basis (data not shown), the model explains a large fraction of the variation in the IASI O_3 dataset (from ~45% to ~85%) and the *RMSE* are lower than 4.5 DU everywhere (~3 DU on the global average). The relative *RMSE* are less than 1% in almost all situations indicating the absence of bias.

The seasonal distributions of the contribution to the total variations in TOCs from the adjusted harmonic terms and explanatory variables, which account for the "natural" variability, and from the LT term are shown in Fig. 2 (left and right panels, respectively). The crosses in the LT panels indicate that the trend estimate in the grid cell is non-significant in the 95% confidence limits (2σ level) when accounting for the autocorrelation in the noise residual at the end of the elimination procedure. While the large influence of the seasonal variations and of the main drivers - namely ENSO, NAO and QBO - on the IASI O_3 records has been clearly attested in Wespes et al. (2017), we demonstrate with Fig.2 that the LT also contributes considerably to the O_3 variations detected by IASI in the troposphere. The LT contribution generally ranges from 15% to 50%, with the largest values (~30-50%) being observed at mid-high latitudes of the S.H. (30°S-70°S) and of the N.H. (~45°N-70°N) in summer. In the S.H., they are associated with the smallest tropospheric O_3 columns (Fig.1; left panels) and the smallest natural contributions (<25%; left panels), while in the N.H. summer, they interestingly correspond to large TOCs, large natural contributions (~50-60%) and the smallest *RMSE* (<12 % or <3 DU). From the annual regression model, the natural variation and the trend contribute respectively for 30-85% and up to 40% to the total variation in TOCs.

In Fig.3, we further investigate the robustness of the estimated trends by performing sensitivity tests in regions of significant trend contributions (e.g. in the N.H. mid-latitudes in summer; cfr Fig.2). The ~9-year time series of IASI O_3 daily averages (dark blue) along with the results from the seasonal regression model with and without including the LT term in the model (light blue and orange lines, respectively) are represented in the top row panel for one specific location (Fig.3a and b; highlighted by a blue circle in the JJA panel in Fig.4). The second row panel provides the deseasonalised IASI (dark blue line) and fitted time series (calculated by subtracting the adjusted seasonal cycle from the time series) resulting from the adjustment with and without including the LT term in the MLR model (light blue and orange lines, respectively). The differences between the fitted models with and without LT are shown in the third rows (pink lines). They match fairly

Atmos. Chem. Phys. Discuss., https://doi.org/10.5194/acp-2017-904
Manuscript under review for journal Atmos. Chem. Phys.
Discussion started: 23 November 2017

well the adjusted trend over the IASI period (3[d] row panel, grey lines; the trend and the *RMSE* values are also indicated) and the adjustment without LT leads to larger residuals (e.g. $RMSE_{\_JJA\_w/o\_LT}$=3.25 DU *vs*. $RMSE_{\_JJA\_with\_LT}$ =3.14 DU in summer). This result demonstrates the possibility to capture trend information from ~9 years of IASI-MLR with only some compensation effects by the other explanatory variables, contrary to what was observed when considering a shorter period of measurements or a lesser temporal sampling (i.e. monthly dataset; e.g. Wespes et al., 2016). It is also worth to mention that the O_3 changes calculated over the whole IASI dataset in summer are larger than the *RMSE* of the model residuals (increase of 5.39±1.86 DU *vs RMSE* of 3.14 DU), underlying the statistical relevance of trend estimates.

The robustness of the adjusted trend is verified at the global scale in Fig.4 which represents the seasonal distributions of the relative differences in the *RMSE* with and without including LT in the MLR model, calculated as $[(RMSE_{\_w/o\_LT} - RMSE_{\_with\_LT})/RMSE_{\_with\_LT} \times 100]$ (in %). An increase in the *RMSE* when excluding LT from the MLR is observed almost everywhere in regions of significant trend contributions (Fig.2), especially in mid-high latitudes of the S.H. and of the N.H. in summer where it reaches 10%. This result indicates that adjusting LT improves the performance of the model and, hence, that a trend signal is well captured by IASI at a regional scale in the troposphere. From the annual model, the increase in the *RMSE* only reaches 5% at mid-high latitudes of the S.H. (data not shown). In regions of weak or non-significant trend contribution (see crosses in Fig.2), no improvement is logically found.

4 O_3 trend over 2008-2017

4.1 Annual and seasonal trends

The annual and the seasonal distributions of the fitted LT terms which are retained in the annual and the seasonal MLR models by the stepwise elimination procedure are respectively represented in Fig. 5 (a) and (b) (in DU/yr). Generally, the mid-high latitudes of both hemispheres and, more particularly, the N.H. mid-latitudes in summer reveal significant negative trends, while the tropics are mainly characterized by non-significant or weak significant trends. Even if trends in emissions have already been able to qualitatively explain measured tropospheric O_3 trends over specific regions, the magnitude and the patterns of the trends considerably vary between independent measurement datasets (e.g. Cooper et al., 2014; the TOAR report – Tropospheric Ozone Assessment Report: Present-day distribution and trends of tropospheric ozone relevant to climate and global atmospheric chemistry model evaluation, Lead Authors: A. Gaudel and O.R. Cooper – coordinated by the International Global Atmospheric Chemistry Project and available on http://www.igacproject.org/activities/TOAR and submitted to Elementa; and references therein) for the reasons discussed in Section 1 and they are not reproduced by model simulations (e.g. Jonson et al., 2006; Cooper et al., 2010; Logan et al., 2012; Wilson et al., 2012; Hess et al., 2013; and references therein). As a result, interpreting adjusted trends at the global scale remains difficult. Nevertheless, several of the statistically significant features observed in Fig.5 show, interestingly, qualitative consistency with respect to recent published findings:

- The S.H. tropical region extending from the Amazon to tropical eastern Indian Ocean seems to indicate a general increase with an annual trend of ~0.13±0.10 DU/yr (i.e. 1.20±0.93 DU over the IASI measurement period), despite the large IAV in TOCs which characterizes the tropics and which likely explains the high frequency of non-significant trends. Enhanced O_3 levels over that region have already been analysed for previous periods (e.g. Logan et al., 1985, 1986; Fishman et al., 1991; Moxim et al., 2000; Thompson et al., 2000, 2007; Sauvage et al., 2006, 2007; Archibald et al., 2017). For instance, the larger O_3 enhancement of ~0.33±0.23 DU/yr (i.e. 3.1±2.2 DU over the whole IASI period) stretching from southern Africa to Australia over the north-east of Madagascar during the austral winter-spring likely originates from large IAV in the subtropical jet-related stratosphere–troposphere exchanges which have been found to primarily contribute to the tropospheric O_3 trends over that region (Liu et al., 2016; 2017). Nevertheless, this finding should be mitigated by the fact that the trend value in the S.H. tropics is of the same magnitude as the *RMSE* of the regression residuals (~2-4.5 DU; see Fig.1).

- The trends over the South-East Asia are mostly non-significant and vary by season. In spring-summer, some grid cells in India, in mainland China and eastwards downwind China exhibit significant positive trends reaching ~0.45 DU/yr (i.e. ~4.2 DU over the IASI measurement period). This tends to indicate that the tropospheric O_3 increases resulting from the strong positive trend in Asian emissions over the past decades (e.g. Zhao et al., 2013; Cooper et al., 2014; Zhang et al., 2016; Cohen et al., 2017; Tarasick et al., 2017; and references therein) persists through 2008-2017 despite the recent decrease in O_3 precursor emissions recorded in China after 2011 (e.g. Duncan et al., 2016; Krotkov et al., 2016; Miyazaki et al., 2017; Van der A et al. 2017). This would indicate that this decrease is probably too recent/weak to recover the 2008 O_3 levels over the entire region. Note, however, that this finding has to be taken carefully given the large model residuals (*RMSE* of ~2-4 DU; cfr Section 3, Fig.1) over that region. Finally, the large uncertainty in trend estimation over the South-East Asia might reflects the large IAV in biomass-burning emissions and lightning NO_x sources, in addition to the recent changes in emissions.

- The mid- and high latitudes of the S.H. show clear patterns of negative trends, all over the year and in a more pronounced manner during winter-spring, with larger amplitudes than those of the *RMSE* values (~-0.35±0.11 DU/yr on average in the 35°S-65°S band; i.e. a trend amplitude of ~|3.3|±1.0 DU over the studied period *vs* a *RMSE* value of ~2.5 DU). These significant negative trends in the S.H. are hard to explain but, considering the stratospheric contribution into the tropospheric columns (natural and artificial due to the limited IASI vertical sensitivity) in the mid-high latitudes of the S.H. (~40-60%; see supplementary materials in Wespes et al., 2016) and the negative significant trends previously reported from IASI in the UTLS/low stratosphere in the 30°S-50°S band, they could be in line with those derived by Zeng et al. (2017) in the UTLS for a clean rural site of S.H. (Lauder, New Zealand) and which mainly originate from increasing tropopause height and O_3 depleting substances.

- In the N.H., a band-like pattern of negative trends is observed in the 40°N-75°N latitudes covering Europe and North America, especially during summer. Averaged annual trend of –0.37±0.18 DU/yr and summer trend of –0.47±0.16 DU/yr (i.e. –3.42±0.65 DU and -4.31±1.47 DU, respectively, from January 2008 to May 2017) are estimated in that latitudinal band. These trend values are significantly larger than the *RMSE* of the MLR model (<3.5 DU; cfr Section 3, Fig.1). Interestingly, both the annual and summer trends are amplified in comparison with the ones calculated in the N.H. mid-latitudes over the 2008-2013 period of IASI measurements (-0.19±0.05 DU/yr and -0.30±0.10 DU/yr for the annual and the summer trends, respectively, calculated in the 30°N-50°N band; see Wespes et al. (2016)). This finding is in agreement with previous studies which point out a possible leveling off of tropospheric O_3 in summer due to the decline of anthropogenic O_3 precursor emissions observed since 2010-2011 in North America, in Western Europe and also in some regions of China (e.g. Cooper et al., 2010; 2012; Logan et al., 2012; Parrish et al., 2012; Oltmans et al., 2013; Simon et al., 2015; Archibald et al., 2017; Miyazaki et al., 2017). Archibald et al. (2017) recently reported a net decrease of ~5% in the global anthropogenic NO_x emissions in the 30°N-90°N latitude band, which is consistent with the annual significant negative trend of -0.32±0.18 DU/yr for O_3 estimated from IASI in that band.

4.2 Expected year for trend detection

In this section, we further verify that it is indeed possible to infer, from the studied IASI period, the significant negative trend derived in the 40°N-75°N band in summer (~|0.5| DU/yr on average, see Section 4.1) by determining the expected year from which such a trend amplitude would be detectable at a global scale. This is achieved by estimating the minimum duration (with probability 0.90) of the IASI O_3 measurements that would be required to detect a trend of a specified magnitude, and its 95% confidence level, following the formalism developed in Tiao et al. (1990) and in Weatherhead et al. (1998):

$$N^* \approx \left[\frac{3.3 \cdot \sigma_\varepsilon}{|\tau_{yr}|} \cdot \sqrt{\frac{1+\Phi}{1-\Phi}} \right]^{2/3} \qquad \text{Eq (1)}$$

$$CL_{N^*} = \left[N^* \cdot e^{-B} ; N^* \cdot e^{+B} \right] \qquad \text{Eq (2)}$$

Atmos. Chem. Phys. Discuss., https://doi.org/10.5194/acp-2017-904
Manuscript under review for journal Atmos. Chem. Phys.
Discussion started: 23 November 2017

Where N^* is the number of the required years, σ_ε is the standard deviation of the autoregressive noise residual ε_t, τ_{yr} is the magnitude of the trend per year, Φ is the lag-1 autocorrelation of the noise. The magnitude of the variation and of the autocorrelation in the noise residuals are taken into account for a better precision on the trend estimate. Given that large variance (σ_ε^2) and large positive autocorrelation Φ of the noise induce small signal-to-noise ratio and long trend-like segments in the dataset, respectively, these two parameters increase the number of years that would be required for detecting a specified trend. CL_{N^*} is the 95% confidence limits which is not symmetric around N^* and depends on B, an estimated uncertainty factor calculated as $\frac{4}{3\sqrt{D}}\sqrt{\frac{1+\Phi}{1-\Phi}}$, with D the number of days in the IASI datasets, which accounts for the uncertainty in Φ (the uncertainty in σ_ε being negligible given that only a few years of data are needed to estimate it; cfr Weatherhead et al. (1998)). As a result, based on the available IASI-A and proxies datasets and assuming that the MLR model used in this study is accurate, we estimate, in Fig. 6 (a) and (b), the expected year when an O_3 trend amplitude of |5| DU per decade (i.e. τ_{yr} = |0.5| DU/yr which corresponds to the averaged absolute value of the fitted negative trends in the N.H. summer; see Fig.5b) is detectable, and its associated maximal confidence limit, respectively. The results in Fig. 6 clearly demonstrates the possibility to infer, from the available IASI dataset, such significant trends in the mid- and high latitudes of the N.H. in summer and fall (trend detectable from ~2016-2017 with an uncertainty of ~6-9 months; cfr Fig.6b). On the contrary, the tropical regions and the N.H. in winter-spring would require additional ~ 6 months to 6 years of measurements to detect an amplitude of |0.5| DU/yr (trend significant only from ~ 2017 – 2023 or after depending on the location and the season). Note also that the strongest negative trends (up to -0.85 DU/yr, i.e. τ_{yr} = |0.85| DU/yr, see Fig.5b) observed in specific regions of the N.H. mid-latitudes would only require ~6 years of IASI measurements for being detected. The mid- and high latitudes of the S.H. would require the shortest period of IASI measurement for detecting a specified trend, with only ~7 years ± 6 months of IASI measurements to detect a |0.5| DU/yr trend (trend detectable from ~2015). That band-like pattern in the S.H. corresponds to the region with the weakest IAV and contribution from large-scale dynamical modes of variability in the IASI TOCs (see Section 3, Fig.1 and 2), which translates into small σ_ε^2 and Φ. Note however that an additional few months of IASI data are required to confirm the smaller negative trend of ~-0.35 DU/yr measured on average in the S.H. (see Fig.5; a period ~9 years ± 6 months being necessary to detect a trend amplitude of |3.5| DU/dec). Given that large σ_ε means large noise residual in the IASI data, the regions of short or long required measurement period coincide, as expected, well with the small or high *RMSE* values of the regression residuals (see Section 3, Fig. 1).

Atmos. Chem. Phys. Discuss., https://doi.org/10.5194/acp-2017-904
Manuscript under review for journal Atmos. Chem. Phys.
Discussion started: 23 November 2017

The regions of the longest measurement periods required in the tropics for a trend detection (up to ~16 years of IASI data) correspond to known patterns of widespread high O_3: (a) above intense biomass burnings in Amazonia and eastwards across tropical Atlantic (Logan et al., 1986; Fishman et al., 1991; Moxim et al., 2000; Thompson et al., 2000, 2007; Sauvage et al., 2007), (b) eastwards Africa across the South Indian Ocean which is subject to large variations in the stratospheric influences during the winter-spring austral period (JJA-SON) (Liu et al., 2016; 2017), (c) Eastwards Africa across the North Indian Ocean to India likely due to large lightning NO_x emissions above central Africa during the wet season associated with the northeastward jet conducting a so-called "O_3 river" (Tocquer et al., 2015) and (d) above regions of positive ENSO "chemical" effect in Equatorial Asia/Australia and eastwards above northern and southern tropical regions (Wespes et al., 2016) explained by reduced rainfalls and biomass fires during El Niño conditions (e.g. Worden et al., 2013). In fact, most of these patterns (a, b and d) are closely connected with strong El- Niño events which extend the duration of the dry season and cause severe droughts, producing intense biomass burning emissions, for instance, over South America (e.g. Chen et al., 2011; Lewis et al., 2011) and South Asia/Australia (e.g. Oman et al., 2013; Valks et al., 2014; Ziemke et al., 2015), and which perturb the tropospheric circulation by increasing the transport of stratospheric O_3 into the troposphere (e.g. Voulgarakis et al., 2011; Neu et al., 2014) and the transport of biomass burning air masses to the Indian Ocean (Zhang et al., 2012). In summary, these large-scale indirect ENSO-related variations in tropospheric O_3 and the lightning NO_x impact on O_3, which are not accounted for in the MLR by specific representative proxies, are misrepresented in the regression models. They induce large noise residuals, i.e. large σ_ε, and, hence, extends the time period needed to detect a trend of any given magnitude.

Figure 6, finally, suggest that a long duration is also required, especially in summer, above and east of China to quantify the anthropogenic impact on the local TOC changes: additional 3±1.5 years or 5±1.5 years for a given |5| or |3.5| DU/dec trend are respectively calculated. This result could be explained by large perturbations in TOCs induced by recent decreases after decades of almost constant increases in surface emissions in China (e.g. Cohen et al., 2017; Miyazaki et al., 2017).

4.3 Multi-linear *vs* single linear model

Even if MLR have already been used for extracting trends in stratospheric and total O_3 columns (e.g. Mäder et al., 2007; Frossard et al., 2013; Rieder et al., 2013; Knibbe et al., 2014), single linear regressions (SLR) without discriminating the natural (chemical and dynamical) factors describing the O_3 variability are still commonly used (e.g. Cooper et al., 2014; the TOAR report – Tropospheric Ozone Assessment Report: Present-day distribution and trends of tropospheric ozone relevant to climate and global atmospheric chemistry model evaluation, Lead Authors: A. Gaudel and O.R. Cooper – and references therein). They are, however, suspected to contribute to trend biases retrieved between independent measurements. In addition to the time-varying instrumental biases, trend biases can also be related to differences in the spatial and the temporal samplings (e.g. Doughty et al., 2011; Saunois et al., 2012; Lin et al., 2015) and in the vertical sensitivity of the measurements. The later artificially alters the characteristics of the sounded layer by contaminations from the above and the below layers leading to a mixing of the trend but also of the natural characteristics originating from these different layers (e.g. troposphere and stratosphere). The differences in the studied period and in the spatio-temporal sampling might also imply differences in the natural influence on the measured O_3 variations. While the impact of the natural contribution is taken into account in the MLR model, it might introduce an additional bias in the trend determined from SLR, making further challenging to compare trends estimated from a series of independent measurements.

The limitation in using a SLR instead of a MLR model for determining trends is explored here by comparing the seasonal distributions of the trends estimated from MLR (see Fig. 5 (b) in Section 4.1.) and from SLR (presented in Fig.7). The highest differences in the fitted trends derived from the two methods are found in the tropics and in some regions of the mid-latitudes of the N.H. They likely result from overlaps between the LT term and other covariates. For instance, the regions of the high significant SLR trends (~0.3-0.5 DU/yr over the tropical western and middle Pacific) during the period extending from September to May match the regions of strong El Niño/Southern Oscillation influence (cfr Fig. 8 and 12 in Wespes et al., 2016). On the contrary, the MLR model lends generally weak significant negative or non-significant trends in the Pacific Niño region during that period and it would even need additional ~3 to 4 years of IASI measurements for detecting the fitted SLR trends (see Section above). The effect of ENSO in overestimating the fitted SLR trend is further illustrated on Fig. 8 which represents the time series of O_3 observed by IASI and adjusted by the annual MLR model (top row) along with the deseasonalized times series (middle row) and the fitted SLR and MLR trends (bottom row). The fitted signal of the ENSO proxy from the MLR regression (calculated as $x_j X_{norm,j}$ following Wespes et al. (2017)) is also represented (bottom row). That example clearly shows that the ENSO influence is considerably compensated by the adjustment of the linear trend in the SLR regression (annual trend of -0.29±0.028 DU/yr from SLR vs -0.13±0.092 DU/yr from MLR for that example). Finally, differences between the SLR and the MLR models are also observed in the region of strong positive NAO influence over the Icelandic/Arctic region during MAM (see Wespes et al. (2016) for a description of the NAO-related O_3 changes). On the contrary, the sub-tropical S.H. exhibit similar seasonal patterns of negative trends from both the SLR and the MLR. It results from the weak natural IAV and contributions in tropospheric O_3 above that region (see Section 3, Fig. 1 and 2), which, hence, limits the compensation effects.

In summary, if considering a long period of measurements is usually recommended in SLR study to pass over the dynamical cycles and, hence, to help in discriminating their influences from trends, we show that it is not accurate enough considering that some dynamics have irregular or no particular periodicity (e.g. NAO, ENSO). Furthermore, accurate satellite measurements of tropospheric O_3 at a global scale are quite recent, limiting the period of available and comparable datasets (e.g. Payne et al., 2017). As a consequence, we support here that using a reliable multivariate regression model based on geophysical parameters and adapted for each specific sounded layer is a robust method for differentiating a "true" trend from any other sources of variability and, hence, that it should help in resolving trend differences between independent datasets.

4.4 Continental influence

In this section, we use the capabilities of IASI to simultaneously measure O_3 and CO in order (1) to differentiate tropospheric and stratospheric air masses, (2) to identify the regions influenced by the continental export/intercontinental transport of O_3 pollution and (3) to evaluate that continental influence on tropospheric O_3 trends as observed by IASI. Similar tracer correlations between CO and O_3 have already been used to give insight into the photochemical O_3 enhancement in air pollution transport (e.g. Parrish et al., 1993; Bertschi et al., 2005). However, there are only a few studies using global satellite data for this purpose (Zhang et al., 2006; Voulgarakis et al., 2010; Kim et al., 2013) and the analysis of the O_3-CO relationship for better understanding the origin of O_3 trends in the troposphere has, to the best of our knowledge, never been explored.

We provide in Fig.9a and 9b the seasonal patterns of the O_3-CO correlations (referred as $R_{O3\text{-}CO}$) and of the dO_3/dCO regression slopes calculated in the troposphere (from the surface to 300 hPa) over the studied IASI period (January 2008 – May 2017). The dO_3/dCO regression slopes, which represent the so-called O_3-CO enhancement ratio, is used to evaluate the photochemical O_3 production in continental outflow regions. The $R_{O3\text{-}CO}$ and the dO_3/dCO distributions are similar and clearly show regional and seasonal differences in the strength of the O_3-CO relationships. Regions of positive and negative correlations allows to discriminate air masses characterized by photochemical O_3 production from precursors (including CO) or CO destruction (both identified by positive $R_{O3\text{-}CO}$) from those characterized by O_3 loss (chemical destruction or surface deposition) or by strong stratospheric contaminations (both identified by negative $R_{O3\text{-}CO}$). Negative $R_{O3\text{-}CO}$ and dO_3/dCO are measured in the high latitudes of both hemispheres all over the year, but more specifically at high latitudes of the S.H. in summer-fall (with $R_{O3\text{-}CO}$ <-0.25 on averages in DJF and MMA). If the high latitudes experience more O_3 destruction than the low latitudes due to a lack of sunlight, the negative correlations for the high latitude regions might also reflect air masses originating from/characterizing the stratosphere due to natural intrusion or to artificial mixing with the troposphere introduced by the limited vertical sensitivity of IASI in the highest latitudes (see Wespes et al., 2016). These processes are likely at the origin of the band-like pattern of negative trends in the S.H. discussed in Sections 3 and 4.1. Negative $R_{O3\text{-}CO}$ and dO_3/dCO are also found above the Caribbean, the Arabic Peninsula and the North Indian Ocean in

Atmos. Chem. Phys. Discuss., https://doi.org/10.5194/acp-2017-904
Manuscript under review for journal Atmos. Chem. Phys.
Discussion started: 23 November 2017

Atmospheric Chemistry and Physics
Discussions

JJA/SON and the South Atlantic in DJF. They are in line with Kim et al. (2013) and they likely reflect the influence of lightning NO_x which produce O_3 but also OH oxidizing CO (e.g. Sauvage et al., 2007; Labrador et al., 2004).

Strong positive correlations are identified in both $R_{O3\text{-}CO}$ and dO_3/dCO patterns over the tropical regions and for mid-latitudes of both Hemispheres during the peak of photochemistry in summer. Maxima ($R_{O3\text{-}CO}$ >0.8 and dO_3/dCO>0.5) are detected in continental pollution outflow regions in the N.H., especially downwind South-East Asia and over the South Africa/Amazonia/South Atlantic region. These O_3-CO correlation patterns from IASI are fully consistent with those measured by TES (Zhang et al., 2006; 2008; Voulgarakis et al., 2010) and by OMI/AIRS (Kim et al., 2013), which have been interpreted with global CTM's as originating from Asian pollution influence and from combustion sources including biomass burning, respectively. The high positive $R_{O3\text{-}CO}$ found in JJA at mid-latitudes of the N.H. are detected in a lesser extent in DJF reflecting the decreasing photochemistry. It is also worth to point out in Fig. 9 the clear hemispheric differences in the $R_{O3\text{-}CO}$ and dO_3/dCO values at mid-high latitudes and, more particularly, the shift of positive $R_{O3\text{-}CO}$ and dO_3/dCO towards higher latitudes of the N.H. during summer (e.g. $R_{O3\text{-}CO}$= 0.24 in summer *vs* 0.038 in spring in the 35°N-55°N band). As a consequence, these results suggest that the band-like pattern of negative trends measured by IASI in summer might substantially reflect the continental pollution influence and, hence, that it could result from the decline of anthropogenic O_3 precursor emissions. Nevertheless, interpreting O_3-CO correlations in the free troposphere, especially in photochemically aged pollution plumes far from the emission sources towards the highest latitudes, remains complicated by mixing of continental combustion outflow with stratospheric air masses, in addition to background dynamic and photochemistry (e.g. Liang et al., 2007).

Finally, we also provide in Fig.9c global patterns of O_3-CO covariances ($COV_{O3\text{-}CO}$). They confirm the band-like pattern of the weak natural variation captured in the mid-latitudes S.H. (see Sections 3 and 4.1) and help identifying the region downwind East China, the northern mid-latitudes pollution outflow and the South tropical region as the ones with the highest pollution variability, in addition to the strongest O_3-CO correlations. Finally, the particularly strong positive O_3-CO relationship in terms of $R_{O3\text{-}CO}$, dO_3/dCO and $COV_{O3\text{-}CO}$ measured over and downwind North India/East China in summer in comparison with the one measured downwind East US and over Europe indicate that the South-East Asia experiences the most of the intense pollution episodes ($COV_{O3\text{-}CO} > 40\times10^{33}$ $mol^2.cm^{-4}$) with the largest O_3 enhancement ($dO_3/dCO > 0.5$) over the last decade, explaining the significant increase in IASI O_3 levels (see Section 4.1) despite the net decrease in O_3 precursor emissions recorded in China after 2011 (e.g. Cohen et al., 2017; Miyazaki et al., 2017).

5 Conclusions

In this study, we have explored, for the first time, the possibility to infer significant trends in tropospheric O_3 from the first ~10 years (January 2008 – May 2017) of the IASI daily measurements at a global scale. To this end, MLR analyses have been performed by applying a multivariate regression model (annual and seasonal formulations), including a linear trend term in addition to chemical and dynamical proxies, on gridded mean tropospheric ozone time series. This work follows on the analysis of the main dynamical drivers of O_3 variations measured by IASI, which was recently published in Wespes et al. (2017). We have first verified the performance of the MLR models in explaining the variations in daily time series over the whole studied period. In particular, we have shown that the model reproduces a large part of the O_3 variations (>70%) with small residuals errors (*RMSE* of ~10%) in the northern latitudes in summer. We have then performed O_3 trend sensitivity tests to verify the possibility to capture trend characteristics independently from natural variations. Despite the weak contribution from the trend to the total variation in TOCs at the global scale, the results demonstrate the possibility to discriminate significant trends from the explanatory variables, especially in summer at mid-high latitudes of the N.H. (~45°N-70°N) where the contribution and the sensitivity of the trend are the largest (contribution of ~30-50% and a ~10% increase in the *RMSE* excluding the LT in the model). We then focused on the interpretation of the global trend estimates. We have found an interesting significant positive trends in the S.H. tropical region extending from the Amazon to the tropical eastern Indian Ocean and over South-East Asia in spring-summer which should however be carefully considered given the high *RMSE* of the regression residuals in these regions. The MLR analysis reveals a band-like pattern of high significant negative trends in the N.H. mid-high latitudes in summer (–0.47±0.16 DU/yr on average in the 45°N-70°N band). The statistical significance of such trend estimates is further verified by estimating, based on the autocorrelation and on the variance of the noise residuals, the minimum number of years of IASI measurements that are required to detect a trend of a |5| DU/dec magnitude. The results clearly demonstrate the possibility to determine such a trend amplitude from the available IASI dataset and the used MLR model at northern mid-high latitudes in summer, while much larger measurement periods are necessary elsewhere. In particular, the regions of the longest required period highlight, in the tropics, a series of known processes that are closely related to the El-Niño dynamic, which underlies the lack of associated parameterizations in the MLR model. The importance of using reliable MLR models in understanding large-scale O_3 variations and in determining trends is further explored by comparing the trends inferred from MLR and SLR, the latter being still commonly used by the international community. The comparison has clearly highlighted the gain of MLR in attributing the trend-like segments in natural variations, such as ENSO, to the right processes and, hence, in avoiding misinterpretation of "apparent" trends in the measurement datasets. Finally, by exploiting the simultaneous and vertically-resolved O_3 and CO measurements from IASI, we have provided and used the O_3-CO correlations in the troposphere to help in determining the origins/characteristics of the air masses with negative or positive trends. The distributions have allowed us to identify, in particular, strong positive O_3-CO correlations, regression slopes and covariance in the N.H. mid-latitudes and northward during summer, which suggests a continental pollution influence in the N.H. band-like pattern of high significant negative trends recorded by IASI and, hence, a direct effect of the policy measures taken to reduce emissions of O_3 precursor species.

This study supports overall the importance of using high density and long term satellite records, such as those provided by IASI, for accurately determining trends in tropospheric O_3 - as required by the scientific community e.g. in the Intergovernmental Panel on Climate Change (IPCC, 2013) - and for further resolving trend biases between independent datasets (Payne et al., 2017; the TOAR report – Tropospheric Ozone Assessment Report: Present-day distribution and trends of tropospheric ozone relevant to climate and global atmospheric chemistry model evaluation, Lead Authors: A. Gaudel and O.R. Cooper). Determination, with IASI, of robust trends at the global scale in tropospheric O_3 will be achievable in the near future by merging the homogeneous O_3 profiles from the three successive instruments onboard Metop-A (2006); -B (2012) and –C (2018) platforms and from the IASI-Next Generation onboard the Metop Second Generation series of satellites (Clerbaux and Crevoisier, 2013; Crevoisier et al., 2014). A long record of tropospheric O_3 measurements will be also assured by the Cross-track Infrared Sounder (CrIS) onboard the Joint Polar Satellite System series of satellites.

Acknowledgments

IASI has been developed and built under the responsibility of the Centre National d'Etudes Spatiales (CNES, France). It is flown onboard the Metop satellites as part of the EUMETSAT Polar System. The IASI L1 data are received through the EUMETCast near real time data distribution service. We acknowledge the financial support from the ESA O_3-CCI, Copernicus O_3-C3S and Eumetsat AC SAF projects. The research in Belgium is also funded by the Belgian State Federal Office for Scientific, Technical and Cultural Affairs and the European Space Agency (ESA Prodex IASI Flow and AC SAF).

Atmos. Chem. Phys. Discuss., https://doi.org/10.5194/acp-2017-904
Manuscript under review for journal Atmos. Chem. Phys.
Discussion started: 23 November 2017

Atmospheric Chemistry and Physics
Open Access
Discussions

Figure captions

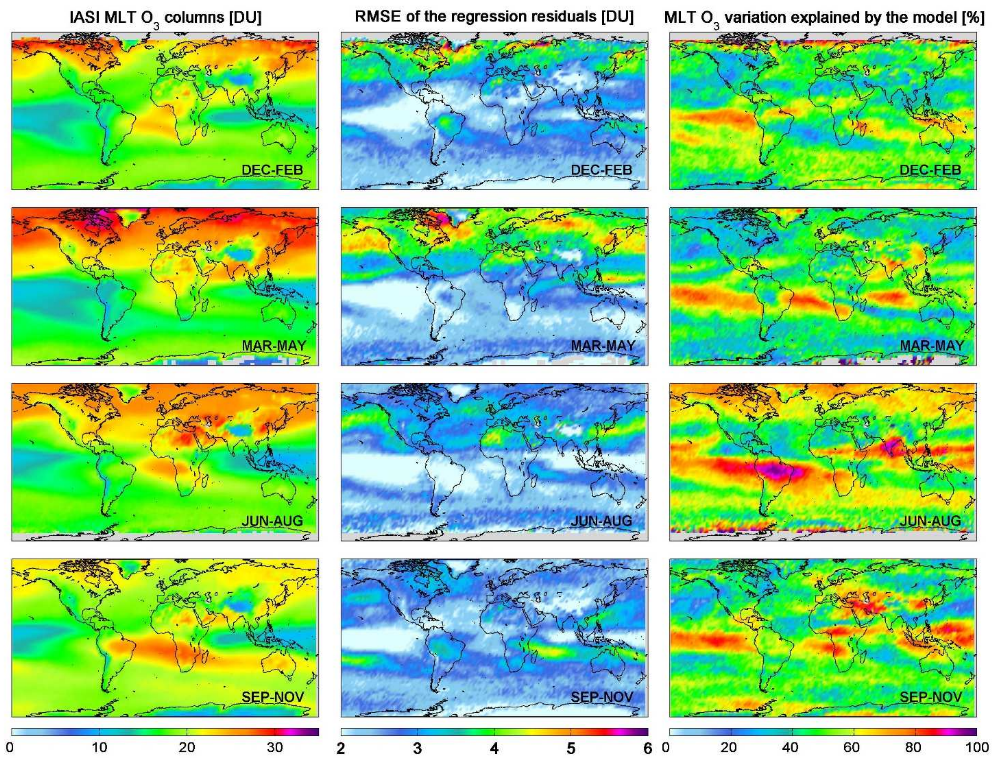

Fig.1. Seasonal distribution of O_3 tropospheric columns (in DU, integrated from ground to 300hPa) measured by IASI and averaged over January 2008 – May 2017 (left panel), of the *RMSE* of the regression fits (in DU, middle panel) and of the fraction of the variation in IASI data explained by the regression model, calculated as $\left[100\times\left(\sigma\left(O_3^{Fitted\_model}(t)\right)/\sigma\left(O_3(t)\right)\right)\right]$ (in %, right panel). Data are averaged over a 2.5°x2.5° grid box.

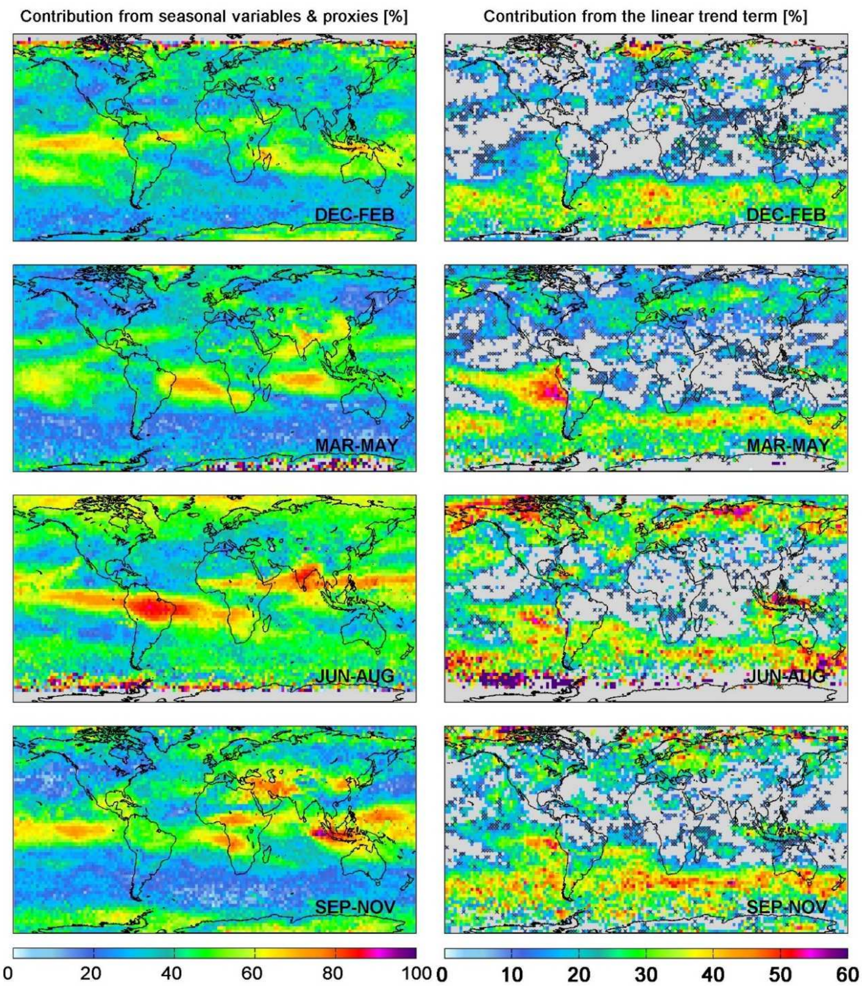

Fig.2. Seasonal distributions of the contribution from the seasonal and explanatory variables into the IASI O_3 variations estimated as $\left[100\times\sigma\left(\sum_{n=1;\,j=2}^{4;m}[a_n;b_n;x_j][\cos(n\omega t);\sin(n\omega t);X_{norm,j}]\right)\Big/\sigma(O_3(t))\right]$ (in %, left panels) and of the contribution from the linear trend calculated as $\left[100\times\sigma\left(x_{j=1}\cdot trend\right)/\sigma(O_3(t))\right]$ (in %, right panels). The grey areas and crosses refer to the non-significant grid cells in the 95% confidence limits (2σ level). Note that the scales are different.

Atmos. Chem. Phys. Discuss., https://doi.org/10.5194/acp-2017-904
Manuscript under review for journal Atmos. Chem. Phys.
Discussion started: 23 November 2017

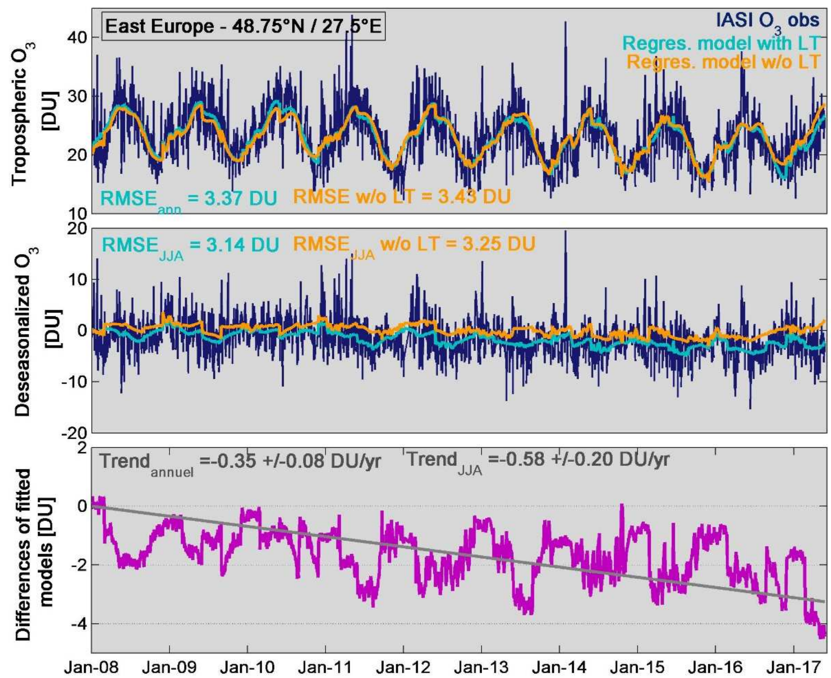

Fig.3. Examples of daily time series of IASI O_3 measurements (dark blue) and of the fitted seasonal regression models with (light blue) and without (orange) the linear term in the troposphere (1st row). Daily time series of the deseasonalised O_3 (observations and regression models; 2d row) and of the difference of the fitted models with and without the linear trend term as well as the adjusted annual trend (pink and grey lines, respectively; 3d row) (given in DU). The *RMSE* (annual and for the JJA period in DU) and the trend values (annual and for the JJA period in DU/yr) are also indicated.

Atmos. Chem. Phys. Discuss., https://doi.org/10.5194/acp-2017-904
Manuscript under review for journal Atmos. Chem. Phys.
Discussion started: 23 November 2017

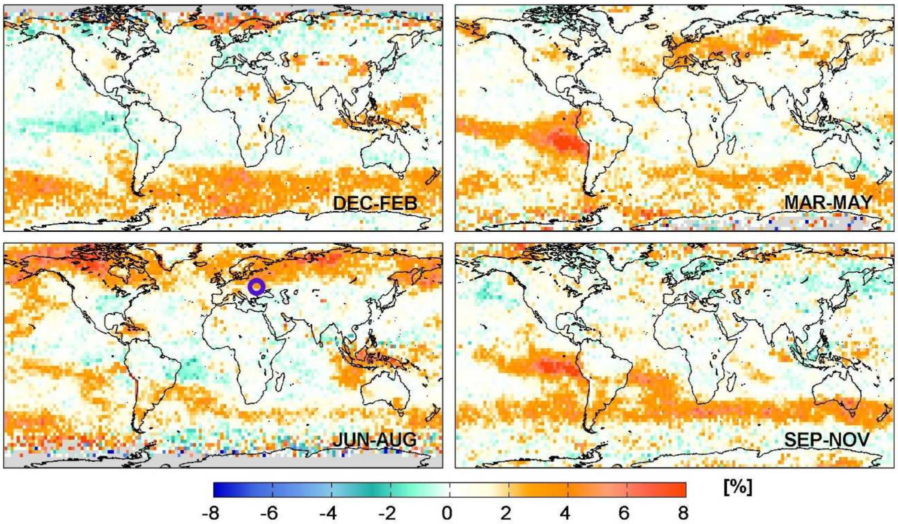

Fig.4. Seasonal distribution of the differences between the *RMSE* of the regression fits with and without linear trend term [$(RMSE_{\_w/o\_LT} - RMSE_{\_with\_LT})/RMSE_{\_with\_LT} \times 100$] (in %). The blue circles in the JJA panel refer to the case presented in Fig.3.

Atmos. Chem. Phys. Discuss., https://doi.org/10.5194/acp-2017-904
Manuscript under review for journal Atmos. Chem. Phys.
Discussion started: 23 November 2017

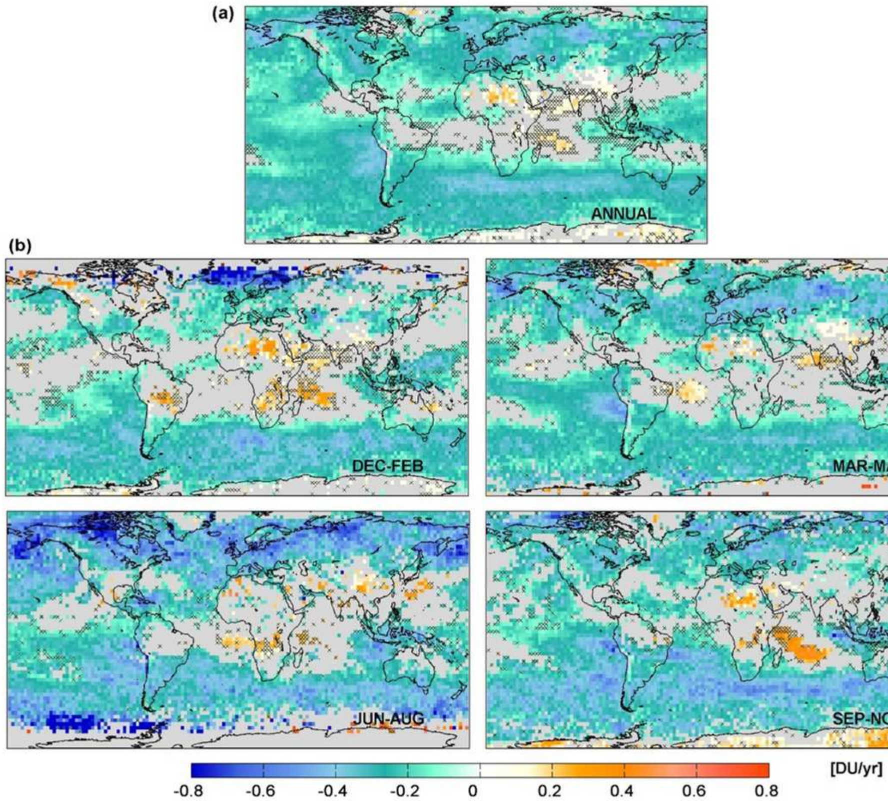

Fig.5. (a) Annual and (b) seasonal distributions of the adjusted trends in DU/yr from the multi-linear regression models. The grey areas and crosses refer to the non-significant grid cells in the 95% confidence limits (2σ level).

Atmos. Chem. Phys. Discuss., https://doi.org/10.5194/acp-2017-904
Manuscript under review for journal Atmos. Chem. Phys.
Discussion started: 23 November 2017

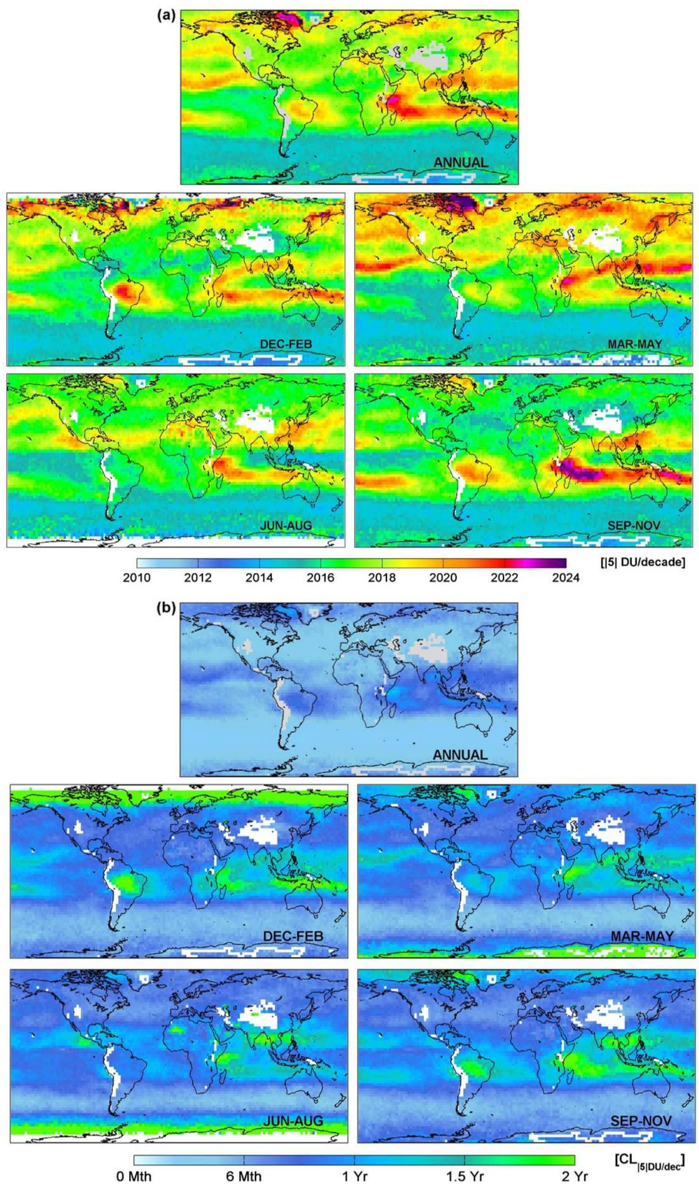

Fig.6 (a) Estimated year of tropospheric IASI O_3 trend detection (with a probability of 90%) for a given trend of |5| DU per decade starting at the beginning of the studied period (20080101) and (b) associated maximal confidence limits from the annual (top panel) and the seasonal (bottom panels) regression models.

Atmos. Chem. Phys. Discuss., https://doi.org/10.5194/acp-2017-904
Manuscript under review for journal Atmos. Chem. Phys.
Discussion started: 23 November 2017

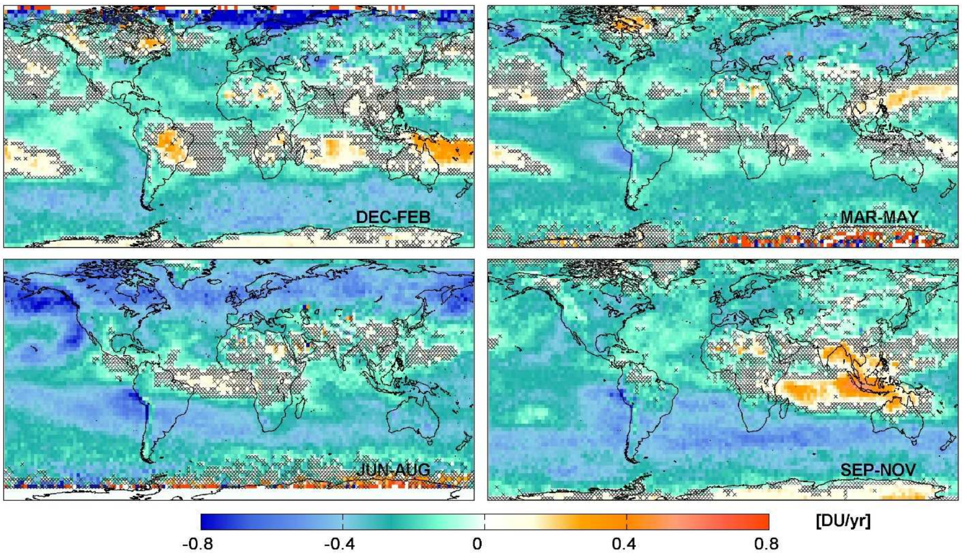

Fig.7. Seasonal distributions of the fitted linear term trends (given in DU/yr) derived from a single linear regression model. The crosses refer to the non-significant grid cells in the 95% confidence limits (2σ level).

Atmos. Chem. Phys. Discuss., https://doi.org/10.5194/acp-2017-904
Manuscript under review for journal Atmos. Chem. Phys.
Discussion started: 23 November 2017

Atmospheric Chemistry and Physics
Open Access
Discussions

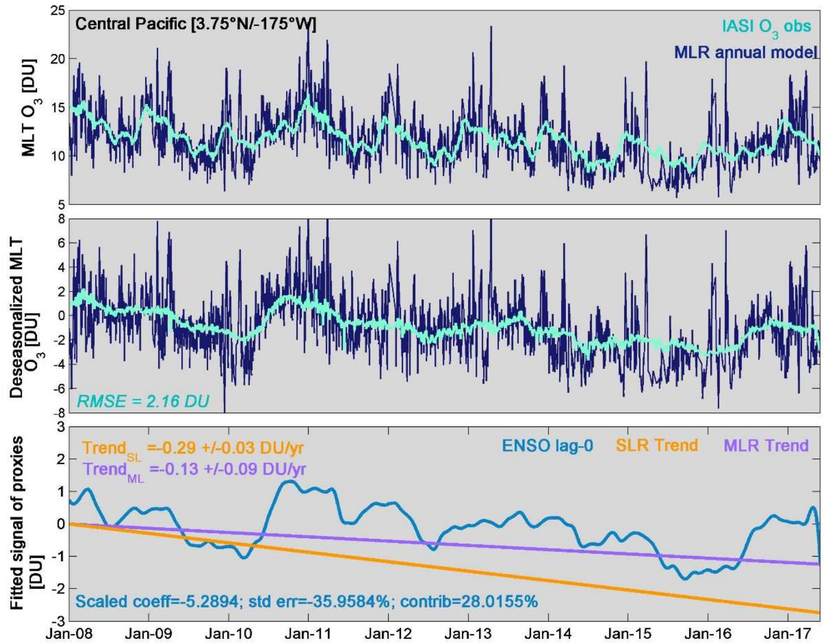

Fig.8. Daily time series of O_3 measured by IASI and adjusted by the multivariate annual regression model (top row and middle row for the deseasonalized O_3), along with the adjusted trends derived from the single and the multivariate linear regressions (SLR and MLR) and of the fitted signal of ENSO proxy (one of the main retained proxies in the multivariate regression model) calculated as $[x_j X_{norm,j}]$ (bottom row) over the equatorial central Pacific (negative ENSO "dynamical" effect) (given in DU). The *RMSE* of the multivariate regression fit and the fitted SLR and MLR trend values are also indicated.

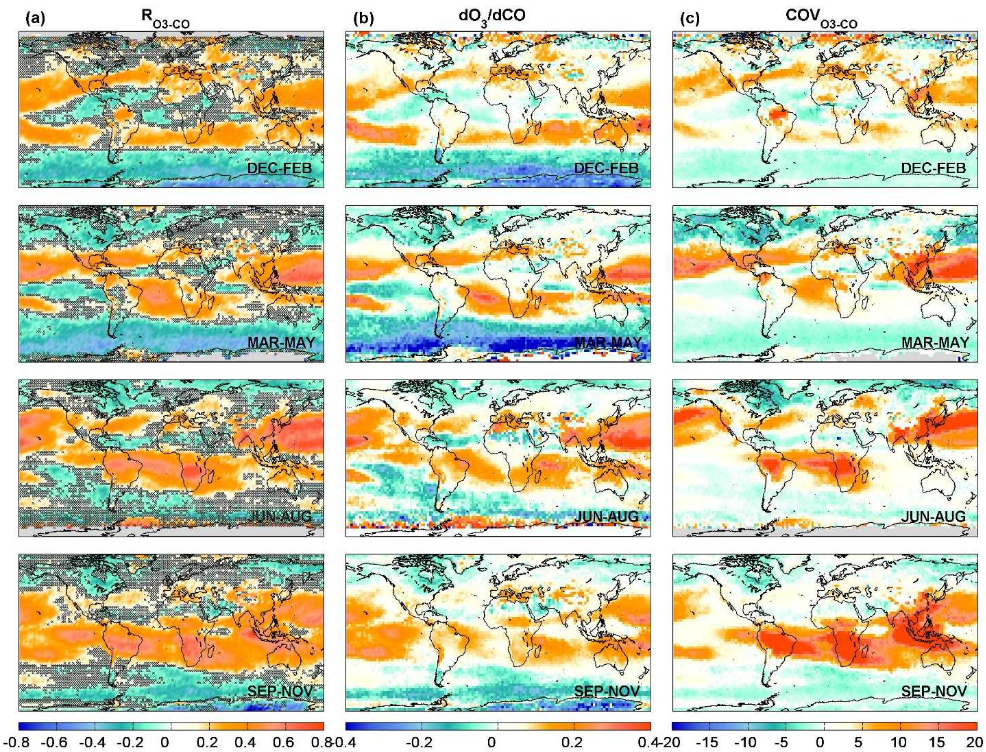

Fig.9. Global distributions of (a) the correlation coefficients ($R_{O3\text{-}CO}$), (b) the regression slope (dO_3/dCO in mol.cm^{-2}/mol.cm^{-2}) and (c) the covariances ($COV_{O3\text{-}CO}$ in 10^{33} mol.cm^{-2}×mol.cm^{-2}) of daily median IASI tropospheric O_3 and CO over January 2008 – May 2017. Data are averaged over a 2.5°x2.5° grid box. Crosses in $R_{O3\text{-}CO}$ panels (a) refer to the non-significant grid cells in the 95% confidence intervals (2σ level).

References

Anton, M., D. Loyola, C. Clerbaux, M. Lopez, J. Vilaplana, M. Banon, J. Hadji-Lazaro, P. Valks, N. Hao, W. Zimmer, P. Coheur, D. Hurtmans, and L. Alados-Arboledas: Validation of the Metop-A total ozone data from GOME-2 and IASI using reference ground-based measurements at the Iberian peninsula, Remote Sensing of Environment, 115, 1380-1386, 2011.

Archibald, A., Y. Elshorbany et al.: Tropospheric Ozone Assessment Report: Critical review of the present-day and near future tropospheric ozone budget, Elem. Sci. Anth., in-review, 2017.

Bertschi, I. T. and Jaffe, D. A.: Long-range transport of ozone, carbon monoxide, and aerosols to the NE Pacific troposphere during the summer of 2003: Observations of smoke plumes from Asian boreal fires, J. Geophys. Res., 110(D5), D05303, doi:10.1029/2004JD005135, 2005.

Boynard, A., D. Hurtmans, M. Koukouli, et al.: Seven years of IASI ozone retrievals from FORLI: validation with independent total column and vertical profile measurements, Atmos. Meas. Tech., 9, 4327-4353, 2016.

Boynard, A., D. Hurtmans, K. Garane, F. Goutail, J. Hadji-Lazaro, M. E. Koukouli, C. Wespes, A. Keppens, J.-P. Pommereau, A. Pazmino, D. Balis, D. Loyola, P. Valks, S. Hassinen, P.-F. Coheur and C. Clerbaux, Validation of the IASI FORLI/Eumetsat O_3 products using satellite (GOME-2), ground-based (Brewer-Dobson, SAOZ) and ozonesonde measurements, in preparation for this QOS special issue.

Chen, Y., Randerson, J. T., Morton, D. C., DeFries, R. S., Collatz, G. J., Kasibhatla, P. S., iglio, L., Jin, Y., and Marlier, M. E.: Forecasting Fire Season Severity in South America Using Sea Surface emperature Anomalies, Science, 334, 787–791, doi:10.1126/science.1209472, 2011.

Clarisse, L., Y. R'Honi ; P.-F. Coheur ; D. Hurtmans, and C. Clerbaux : Thermal infrared nadir observations of 24 atmospheric gases. Geophysical Research Letters, 38, L10802, 2011.

Clerbaux, C., A. Boynard, L. Clarisse, M. George, J. Hadji-Lazaro, H. Herbin, D. Hurtmans, M. Pommier, A. Razavi, S. Turquety, C. Wespes, and P.-F. Coheur: Monitoring of atmospheric composition using the thermal infrared IASI/MetOp sounder, Atmos. Chem. Phys., 9, 6041-6054, 2009.

Clerbaux C. and C. Crevoisier: New Directions: Infrared remote sensing of the troposphere from satellite: Less, but better, Atmospheric Environment, 72, 24-26, 2013.

Crevoisier, C., Clerbaux, C., Guidard, V., Phulpin, T., Armante, R., Barret, B., Camy-Peyret, C., Chaboureau, J.-P., Coheur, P.-F., Crépeau, L., Dufour, G., Labonnote, L., Lavanant, L., Hadji-Lazaro, J., Herbin, H., Jacquinet-Husson, N., Payan, S., Péquignot, E., Pierangelo, C., Sellitto, P., and Stubenrauch, C. : Towards IASI-New Generation (IASI-NG): impact of improved spectral resolution and radiometric noise on the retrieval of thermodynamic, chemistry and climate variables, Atmos. Meas. Tech., 7, 4367-4385, 2014.

Cohen, Y., et al.: Climatology and long-term evolution of ozone and carbon monoxide in the UTLS at northern mid-latitudes, as seen by IAGOS from 1995-2013, ACPD, in-review, 2017.

Cooper, O., D. Parrish, A. Stohl, M. Trainer, P. Nédélec, V. Thouret, J.-P. Cammas, S. Oltmans, B. Johnson and D. Tarasick: Increasing springtime ozone mixing ratios in the free troposphere over western North America, Nature, 463, 344–348, doi:10.1038/nature08708, 2010.

Cooper, O. R., R.-S. Gao, D. Tarasick, T. Leblanc, and C. Sweeney: Long-term ozone trends at rural ozone monitoring sites across the United States, 1990–2010, *J. Geophys. Res.*, *117*, D22307, doi:10.1029/2012JD018261, 2012.

Cooper, O. R., D. D. Parrish, J. Ziemke, N. V. Balashov, M. Cupeiro, I. E. Galbally, S. Gilge, L. Horowitz, N. R. Jensen, J.-F. Lamarque, V. Naik, S. J. Oltmans, J. Schwab, D. T. Shindell, A. M. Thompson, V. Thouret, Y. Wang, R. M. Zbinden: Global distribution and trends of tropospheric ozone: An observation-based review, Elementa: Science of the Anthropocene, 2, 000029, doi:10.12952/journal.elementa.000029, 2014.

Doughty, D. C., Thompson, A. M., Schoeberl, M. R., Stajner, I., Wargan, K., and Hui, W. C. J.: An intercomparison of tropospheric ozone retrievals derived from two Aura instruments and measurements in western North America in 2006, J. Geophys. Res., 116, D06303,doi:10.1029/2010JD014703, 2011.

Dufour, G., M. Eremenko, A. Griesfeller, B. Barret, E. LeFlochmoen, C. Clerbaux, J. Hadji-Lazaro, P.-F. Coheur, and D. Hurtmans: Validation of three different scientific ozone products retrieved from IASI spectra using ozonesondes, Atmos. Meas. Tech., 5, 611-630, 2012.

Duncan, B. N., Lamsal, L. N., Thompson, A. M., Yoshida, Y., Lu, Z., Streets, D. G., Hurwitz, M. M., and Pickering, K. E.: A space-based, high-resolution view of notable changes in urban NOx pollution around the world (2004-2005), J. Geophys. Res. 121, 976–96, 2016.

Fishman, J., K. Fakhruzzaman, B. Cros and D. Nganda: Identification of widespread pollution in the southern-hemisphere deduced from satellite analyses, Science, 252, 1693-1696, 1991.

Fishman, J., Creilson, J. K., Wozniak, A. E., and Crutzen, P. J.: Interannual variability of stratospheric and tropospheric ozone determined from satellite measurements, J. Geophys. Res., 110, D20306, doi:10.1029/2005JD005868, 2005.

Frossard, L., H.E. Rieder, M. Ribatet, J. Staehelin, J. A, Maeder, S. Di Rocco, A. C. Davison, T. Pete.: On the relationship between total ozone and atmospheric dynamics and chemistry at mid-latitudes – Part 1: Statistical models and spatial fingerprints of atmospheric dynamics and chemistry, Atmos. Chem. Phys., 13, 147–164, doi:10.5194/acp-13-147-2013, 2013.

Fusco, A. C., and J. A. Logan: Analysis of 1970–1995 trends in tropospheric ozone at northern hemisphere midlatitudes with the GEOSCHEM model, J. Geophys. Res., 108(D15), 4449, doi:10.1029/2002JD002742, 2003.

Gaudel, A., O. R. Cooper, G. Ancellet, B. Barret, A. Boynard, J. P. Burrows, C. Clerbaux, P.-F. Coheur, J. Cuesta, E. Cuevas, S. Doniki, G. Dufour, F. Ebojie, G. Foret, O. Garcia, M. J. Granados-Muñoz, J. Hannigan, F. Hase, B. Hassler, G. Huang, D. Hurtmans, D. Jaffe, N. Jones, P. Kalabokas, B. Kerridge, S. Kulawik, B. Latter, T. Leblanc, E. Le Flochmoën, W. Lin, J. Liu, X. Liu, E. Mahieu, A. McClure-Begley, J. Neu, M. Osman, M. Palm, H. Petetin, I. Petropavlovskikh, R. Querel, N. Rahpoe, A. Rozanov, M. G. Schultz, J. Schwab, R. Siddans, D. Smale, M. Steinbacher, H. Tanimoto, D. Tarasick, V. Thouret, A. M. Thompson, T. Trickl, E. Weatherhead, C. Wespes, H. Worden, C. Vigouroux, X. Xu, G. Zeng, J. Ziemke: Tropospheric Ozone Assessment Report: Present-day distribution and trends of tropospheric ozone relevant to climate and global atmospheric chemistry model evaluation, submitted to Elementa.

Gazeaux, J., C. Clerbaux, M. George, J. Hadji-Lazaro, J. Kuttippurath, P.-F. Coheur, D. Hurtmans, T. Deshler, M. Kovilakam, P. Campbell, V. Guidard, F. Rabier, and J.-N. Thepaut: Intercomparison of polar ozone profiles by IASI/Metop sounder with 2010 concordiasi ozonesonde observations, Atmos. Meas. Tech., 5, 7923-7944, 2012.

Hess, P.G. and R. Zbinden: Stratospheric impact on tropospheric ozone variability and trends: 1990–200, Atmos. Chem. Phys., 13, 649–674, 2013.

Hilton, F., R. Armante, T. August, et al. : Hyperspectral Earth Observation from IASI: Five Years of Accomplishments, Bulletin of the American Meteorological Society, vol. 93, issue 3, pp. 347-370, 2012.

Hurtmans, D., P. Coheur, C.Wespes, L. Clarisse, O. Scharf, C. Clerbaux, J. Hadji-Lazaro, M. George, and S. Turquety: FORLI radiative transfer and retrieval code for IASI, Journal of Quantitative Spectroscopy and Radiative Transfer, 113, 1391-1408, 2012.

Intergovernmental Panel on Climate Change, Climate Change 2013: The Physical Science Basis. Contribution of Working Group I to the Fifth Assessment Report of the Intergovernmental Panel on Climate Change, edited by T. F. Stocker et al., pp. 164–270, Cambridge Univ. Press, Cambridge, U. K., and New York, 2013.

Jonson, J. E., Simpson, D., Fagerli, H., and Solberg, S.: Can we explain the trends in European ozone levels?, Atmos. Chem. phys., 6, 51–66, doi:10.5194/acp-6-51-2006, 2006.

Keppens, A., J.-C. Lambert, J. Granville, D. Hubert, T. Verhoelst, S. Compernolle, B. Latter, B. Kerridge, R. Siddans, A. Boynard, J. Hadji-Lazaro, C. Clerbaux, C. Wespes, D. R. Hurtmans, P.-F. Coheur, J. van Peet, R. van der A, K. Garane, M. E. Koukouli, D. S. Balis, A. Delcloo, R. Kivi, R. Stübi, S. Godin-Beekmann, M. Van Roozendael, C. Zehner: Quality assessment of the Ozone_cci Climate Research Data Package (release 2017): 2. Ground-based validation of nadir ozone profile data products, in preparation for this QOS special issue.

Kim, P. S., D. J. Jacob, X. Liu, J. X.Warner, K. Yang, K. Chance, V. Thouret, and P. Nedelec: Global ozone–CO correlations from OMI and AIRS: constraints on tropospheric ozone sources, Atmos. Chem. Phys., 13, 9321–9335, 2013.

Knibbe J. S., R. J. van der A, and A. T. J. de Laat: Spatial regression analysis on 32 years of total column ozone data, Atmos. Chem. Phys., 14, 8461–8482, 2014.

Krotkov, N. A., McLinden, C. A., Li, C., Lamsal, L. N., Celarier, E. A., Marchenko, S. V., Swartz, W. H., Bucsela, E. J., Joiner, J., Duncan, B. N., Boersma, K. F., Veefkind, J. P., Levelt, P. F., Fioletov, V. E., Dickerson, R. R., He, H., Lu, Z., and Streets, D. G.: Aura OMI observations of regional SO_2 and NO_2 pollution changes from 2005 to 2015, Atmos. Chem. Phys., 16, 4605-4629, doi:10.5194/acp-16-4605-2016, 2016.

Labrador, L. J., von Kuhlmann, R., and Lawrence, M. G.: Strong sensitivity of the global mean OH concentration and the tropospheric oxidizing efficiency to the source of NOx from lightning, Geophys. Res. Lett., 31, L06102, doi:10.1029/2003GL019229, 2004.

Lewis, S. L., Brando, P. M., Phillips, O. L., van der Heijden, G. M. F., and Nepstad, D.: The 2010 Amazon Drought, Science, 331, 554–554, doi:10.1126/science.1200807, 2011.

Liang, Q., Jaegle, L., Hudman, R. C., Turquety, S., Jacob, D. J., Avery, M. A., Browell, E. V., Sachse, G. W., Blake, D. R., Brune, W., Ren, X., Cohen, R. C., Dibb, J. E., Fried, A., Fuelberg, H., Porter, M., Heikes, B. G., Huey, G., Singh, H. B., andWennberg, P. O.: Summertime influence of Asian pollution in the free troposphere over North America, J. Geophys. Res., 112, D12S11, doi:10.1029/2006JD007919, 2007.

Lin, M., L. W. Horowitz, O. R. Cooper, D. Tarasick, S. Conley, L. T. Iraci, B. Johnson, T. Leblanc, I. Petropavlovskikh, and E. L. Yates: Revisiting the evidence of increasing springtime ozone mixing ratios in the free troposphere over western North America, Geophys. Res. Lett., 42, 8719–8728, doi:10.1002/2015GL0653112015.

Liu, X., P. K. Bhartia, K. Chance, R. J. D. Spurr, and T. P. Kurosu: Ozone profile retrievals from the Ozone Monitoring Instrument, Atmos. Chem. Phys., 10, 2521–2537, 2010.

Liu, J., Rodriguez, J. M., Thompson, A. M., Logan, J. A., Douglass, A. R., Olsen, M. A., Steenrod, S. D., and Posny, F.: Origins of tropospheric ozone interannual variation over Reunion: A model investigation, J. Geophys. Res.-Atmos., 121, 521–537, doi:10.1002/2015jd023981, 2016.

Liu, J., et al.: Causes of interannual variability over the southern hemispheric tropospheric ozone maximum, Atmos. Chem. Phys., 17, 3279–3299, 2017.

Logan, J. A., M. J. Prather, S. C. Wofsy, and M. B. McElroy: Tropospheric chemistry: A global perspective, J. Geophys. Res., 86 (NC8), 7210–7254, doi:10.1029/JC086iC08p07210, 1981.

Atmos. Chem. Phys. Discuss., https://doi.org/10.5194/acp-2017-904
Manuscript under review for journal Atmos. Chem. Phys.
Discussion started: 23 November 2017

Atmospheric Chemistry and Physics
Open Access
Discussions

Logan, J. A.: Tropospheric Ozone: Seasonal behaviour, Trends, and Anthropogenic Influence, J. Geophys. Res., 90(D6), 10 463–10 482, 1985.

Logan, J. A., and V. W. J. H. Kirchhoff: Seasonal variations of tropospheric ozone at Natal, Brazil, J. Geophys. Res., 91(D7), 7875–7881, doi:10.1029/JD091iD07p07875, 1986.

Logan, J. A., Staehelin, J., Megretskaia, I. A., Cammas, J.-P., Thouret, V., Claude, H., De Backer, H., Steinbacher, M., Scheel, H.-E., Stübi, R., Fröhlich, M., and Derwent, R.: Changes in ozone over Europe: Analysis of ozone measurements from sondes, regular aircraft (MOZAIC) and alpine surface sites, J. Geophys. Res., doi:10.1029/2011JD016952, 2012.

Mäder, J. A., J. Staehelin, D. Brunner, W.A. Stahel, I. Wohltmann, and T. Peter: Statistical modelling of total ozone: Selection of appropriate explanatory variables, J. Geophys. Res., 112, D11108, doi:10.1029/2006JD007694, 2007.

Miyazaki et al.: Decadal changes in global surface NOx emission from multi-constituent satellite data assimilation, Atmos. Chem. Phys., 17, 807–837, 2017.

Moxim, W. J., and H. Levy II: A model analysis of the tropical South Atlantic Ocean tropospheric ozone maximum: The interaction of transport and chemistry, J. Geophys. Res., 105(D13), 17393–17415, d oi:10.1029/2000JD900175, 2000.

Neu, J.L., T. Flury, G. L. Manney, M. L. Santee, N. J. Livesey and J. Worden, Tropospheric ozone variations governed by changes in stratospheric circulation, Nat. Geosc., 7, 340–344, doi:10.1038/ngeo2138, 2014.

Oetjen, H., Payne, V.H., Kulawik, S.S., Eldering, A., Worden, J., Edwards, D.P., Francis, G.L., Worden, H.M., Clerbaux, C., Hadji-Lazaro, J., Hurtmans, D. : Extending the satellite data record of tropospheric ozone profiles from Aura-TES to MetOp-IASI, Atmos. Meas. Tech., 7, 4223-4236, doi:10.5194/amt-7-4223-2014, 2014.

Oltmans, S.J, A. S. Lefohn; D. Shadwick, J. M. Harris, H.-E. Scheel, I. Galbally, D. W. Tarasick, B. J. Johnson, E.G. Brunke, H. Claude, G. Zeng, S. Nichol, F.J. Schmidlin, J. Davies, E. Cuevas, A. Redondas, H. Naoe, T. Nakano, T. Kawasato: Recent Tropospheric Ozone Changes - A Pattern Dominated by Slow or No Growth, Atmospheric Environment, 67, p. 331-351, 10.1016/j.atmosenv.2012.10.057, 2013.

Oman, L. D., Douglass, A. R., Ziemke, J. R., Rodriguez, J. M., Waugh, D. W., and Nielsen, J. E.: The ozone response to ENSO in Aura satellite measurements and a chemistry–climate simulation, J. Geophys. Res.-Atmos., 118, 965–976, 2013.

Parrington, M., P. I. Palmer, D. K. Henze, D. W. Tarasick, E. J. Hyer, R. C. Owen, D. Helmig, C. Clerbaux, K. W. Bowman, M. N. Deeter, E. M. Barratt, P.-F. Coheur, D. Hurtmans, Z. Jiang, M. George, and J. R. Worden: The influence of boreal biomass burning emissions on the distribution of tropospheric ozone over north America and the north Atlantic during 2010, Atmos. Chem. Phys., 12, 2077-2098, doi: 10.5194/acp-12-2077-2012, 2012.

Parrish, D.D., Holloway, J.S., Trainer, M., Murphy, P.C., Forbes, G.L., and Fehsenfeld, F.C.: Export of North American Ozone Pollution to the North Atlantic Ocean, Science, 259, 1436–1439, 1993.

Parrish, D.D., K.S. Law, J. Staehelin, R. Derwent, O.R. Cooper, et al.: Long-term changes in lower tropospheric baseline ozone concentrations at northern mid-latitudes. Atmos. Chem. Phys 12: 11485–11504. doi:10.5194/acp-12-11485-2012, 2012.

Payne, V. H., J. L. Neu and H. M. Worden: Satellite observations for understanding the drivers of variability and trends in tropospheric ozone, J. Geophys. Res., in-press, 2017.

Pommier, M., C. Clerbaux, K. S. Law, G. Ancellet, P. Bernath, P.-F. Coheur, J. Hadji- Lazaro, D. Hurtmans, P. Nedelec, J.-D. Paris, F. Ravetta, T. B. Ryerson, H. Schlager, and A. J.Weinheimer: Analysis of IASI tropospheric O_3 data over the arctic during POLARCAT campaigns in 2008, Atmos. Chem. Phys., 12, 7371-7389, doi:doi:10.5194/acp-12-7371-2012, 2012.

Rieder, H. E., Frossard, L., Ribatet, M., Staehelin, J., Maeder, J. A., Di Rocco, S., Davison, A. C., Peter, T.,Weihs, P., and Holawe, F.: On the relationship between total ozone and atmospheric dynamics and chemistry at mid-latitudes – Part 2: The effects of the El Nino/Southern Oscillation, volcanic eruptions and contributions of atmospheric dynamics and chemistry to long-term total ozone changes, Atmos. Chem. Phys., 13, 165–179, 2013.

Rodgers, C. D.: Inverse Methods for Atmospheric Sounding: Theory and Practice, World Scientific, Series on Atmospheric, Oceanic and Planetary Physics, 2, Hackensack, N. J., 2000.

Safieddine, S., Boynard, A., Coheur, P.-F., Hurtmans, D., Pfister, G., Quennehen, B., Thomas, J. L., Raut, J.-C., Law, K. S., Klimont, Z., Hadji-Lazaro, J., George, M., and Clerbaux, C.: Summertime tropospheric ozone assessment over the Mediterranean region using the thermal infrared IASI/MetOp sounder and the WRF-Chem model, Atmos. Chem. Phys., 14, 10119–10131, doi:10.5194/acp-14-10119-2014, 2014.

Saunois, M., Emmons, L., Lamarque, J.-F., Tilmes, S., Wespes, C., Thouret, V., and Schultz, M.: Impact of sampling frequency in the analysis of tropospheric ozone observations, Atmos. Chem. Phys., 12, 6757–6773, doi:10.5194/acp-12-6757-2012, 2012.

Sauvage, B., Thouret, V., Thompson, A. M., Witte, J. C., Cammas, J. P., Nedelec, P., and Athier, G.: Enhanced view of the “tropical Atlantic ozone paradox” and “zonal wave one” from the in situ MOZAIC and SHADOZ data, J. Geophys. Res.-Atmos., 111, D01301, doi:10.1029/2005jd006241, 2006.

Sauvage, B., Martin, R. V., van Donkelaar, A., and Ziemke, J. R.: Quantification of the factors controlling tropical tropospheric ozone and the South Atlantic maximum, J. Geophys. Res.-Atmos., 112, D11309, doi:10.1029/2006jd008008, 2007.

Scannell, C., D. Hurtmans, A. Boynard, J. Hadji-Lazaro, M. George, A. Delcloo, A. Tuinder, P.F. Coheur, and C. Clerbaux: Antarctic ozone hole as observed by IASI/MetOp for 2008-2010, Atmos. Meas. Tech., 5, 123-139, 2012.

Simon, H., A. Reff, B. Wells, J. Xing, and N. Frank: Ozone Trends Across the United States over a Period of Decreasing NOx and VOC Emissions, Environ. Sci. Technol., 49, 186−195, dx.doi.org/10.1021/es504514z, 2015.

Stohl, A., S. Eckhardt, C. Forster, P. James, and N. Spichtinger: On the pathways and timescales of intercontinental air pollution transport. J. Geophys. Res. 107 (D23), 4684, doi:10.1029/2001JD001396, 2002.

Thompson, D. W. J. and J.M. Wallace: Annular modes in the extratropical circulation. Part I: month-to month variability, J. Climate, 13, 1000–1016, 2000.

Thompson, A.M., J.C. Witte, H.G.J. Smit, S.J. Oltmans, B.J. Johnson, V.W.J H. Kirchhoff, and F.J. Schmidlin: Southern Hemisphere Additional Ozonesondes (SHADOZ) 1998-2004 tropical ozone climatology: 3. Instrumentation, station-to-station variability, and evaluation with simulated flight profiles, J. Geophys. Res., 112, D03304, doi:10.1029/2005JD007042, 2007.

Tarasick et al.: Tropospheric Ozone Assessment Report: Tropospheric ozone observations, Elem. Sci. Anth., in-review, 2017.

Thouret, V., J.-P. Cammas, B. Sauvage, G. Athier, R. Zbinden, R., P. Nédélec, P. Simon, and F. Karcher: Tropopause referenced ozone climatology and inter-annual variability (1994–2003) from the MOZAIC programme, Atmos. Chem. Phys., 6, 1033–1051, doi:10.5194/acp-6-1033-2006, 2006.

Tiao, G. C., G. C. Reinsel, D. Xu, J. H. Pedrick, X. Zhu, A. J. Miller, J. J. DeLuisi, C. L. Mateer, and D. J. Wuebbles, Effects of autocorrelation and temporal sampling schemes on estimates of trend and spatial correlation, J . GeophysR. es., 95, 20,507-20,517, 1990.

Tocquer, F., Barret, B., Mari, C., Le Flochmoen, E., Cammas, J. P., and Sauvage, B.: An upper tropospheric 'ozone river' from Africa to India during the 2008 Asian post-monsoon season, Tellus B, 67, 25350, doi:10.3402/tellusb.v67.25350, 2015.

Valks, P., N. Hao, S. Gimeno Garcia, D. Loyola, M. Dameris, P. Jöckel, and A. Delcloo: Tropical tropospheric ozone column retrieval for GOME-2, Atmos. Meas. Tech., 7, 2513–2530, doi:10.5194/amt-7-2513-2014, 2014.

Van der A, R. J., et al.: Cleaning up the air: effectiveness of air quality policy for SO_2 and NO_x emissions in China, Atmos. Chem. Phys., 17, 1775–1789, 2017.

Voulgarakis, A., Telford, P. J., Aghedo, A. M., Braesicke, P., Faluvegi, G., Abraham, N. L., Bowman, K. W., Pyle, J. A., and Shindell, D. T.: Global multu-year O_3-CO correlation patterns from models and TES satellite observations, Atmos. Chem. Phys., 11, 5819–5838, doi:10.5194/acp-10-2491-2010, 2010.

Voulgarakis, A., P. Hadjinicolaou, J. A. Pyle: Increases in global tropospheric ozone following an El Nino event: examining stratospheric ozone variability as a potential driver, Atmos. Sci. Let. 12: 228–232, doi: 10.1002/asl.318, 2011.

Weatherhead, E.C., G. C. Reinsel, G. C. Tiao, X.-L. Meng, D. Choi, W.-K. Cheang, T. Keller, J. DeLuisi, D. J. Wuebbles, J. B. Kerr, A. J. Miller, S. J. Oltmans and J. E. Frederick: Factors affecting the detection of trends: Statistical considerations and applications to environmental data, J. Geophys. Res. Atmos., 103, 17149–17161, 1998.

Wespes, C., D. Hurtmans, L.K. Emmons, S. Safieddine, C. Clerbaux, D.P. Edwards, and P.-F. Coheur: Ozone variability in the troposphere and the stratosphere from the first six years of IASI observations (2008-2013), Atmos. Chem. Phys., 16, 5721-5743, 2016.

Wespes, C., D. Hurtmans, C. Clerbaux, and P.-F. Coheur: O3 variability in the troposphere as observed by IASI over 2008–2016 — Contribution of atmospheric chemistry and dynamics, J. Geophys. Res. Atmos., 122, 2429–2451, doi:10.1002/2016JD025875, 2017.

Wilson, R. C., Z.L. Fleming, P.S. Monks, G. Clain, S.Henne, I.B. Konovalov, S. Szopa, and L. Menut: Have primary emission reduction measures reduced ozone across Europe? An analysis of European rural background ozone trends 1996–2005, Atmos. Chem. Phys., 12, 437–454, doi:10.5194/acp-12-437-2012, 2012.

Worden, J., Jiang, Z., Jones, D.B.A., Alvarado, M., Bowman, K., Frankenberg, C., Kort, E.A., Kulawik, S., S., Lee, M., Liu, J., Payne, V., Wecht, K., Worden, H.: El Niño, the 2006 Indonesian peat fires, and the distribution of atmospheric methane, Geophys. Res. Let., V40, 1–6, doi:10.1002/grl.50937, 2013.

Zbinden, R. M., J.-P. Cammas, V. Thouret, P. Nédélec, F. Karcher, and P. Simon: Mid-latitude tropospheric ozone columns from the MOZAIC program: climatology and interannual variability, Atmos. Chem. Phys., 6, 1053–1073, doi:10.5194/acp-6-1053-2006, 2006.

Zeng, G., Morgenstern, O., Shiona, H., Thomas, A. J., Querel, R. R., and Nichol, S. E.: Attribution of recent ozone changes in the Southern Hemisphere mid-latitudes using statistical analysis and chemistry-climate model simulations, Atmos. Chem. Phys. 17, 10495-10513, 2017.

Atmos. Chem. Phys. Discuss., https://doi.org/10.5194/acp-2017-904
Manuscript under review for journal Atmos. Chem. Phys.
Discussion started: 23 November 2017

Zhang, L., Jacob, D. J., Bowman, K. W., Logan, J. A., Turquety, S., Hudman, R. C., Li, Q., Beer, R., Worden, H. M., Worden, J. R., Rinsland, C. P., Kulawik, S. S., Lampel, M. C., Shephard, M. W., Fisher, B. M., Eldering, A., and Avery, M. A.: Ozone-CO correlations determined by the TES satellite instrument in continental outflow regions, Geophys. Res. Lett., 33, L18804, doi:10.1029/2006GL026399, 2006.

Zhang, L., Jacob, D. J., Boersma, K. F., Jaffe, D. A., Olson, J. R., Bowman, K. W., Worden, J. R., Thompson, A. M., Avery, M. A., Cohen, R. C., Dibb, J. E., Flock, F. M., Fuelberg, H. E., Huey, L. G., McMillan, W. W., Singh, H. B., and Weinheimer, A. J.: Transpacific transport of ozone pollution and the effect of recent Asian emission increases on air quality in North America: an integrated analysis using satellite, aircraft, ozonesonde, and surface observations, Atmos. Chem. Phys., 8, 6117–6136, doi:10.5194/acp-8-6117-2008, 2008.

Zhang, L., Li, Q. B., Murray, L. T., Luo, M., Liu, H. and co-authors: A tropospheric ozone maximum over the equatorial Southern Indian Ocean. Atmos. Chem. Phys. 12, 4279-4296, 2012.

Zhang, Y., O. R. Cooper, A. Gaudel, A. M. Thompson, P. Nédélec, S.-Y. Ogino and J. J. West (2016), Tropospheric ozone change from 1980 to 2010 dominated by equatorward redistribution of emissions, *Nature Geoscience*, doi: 10.1038/NGEO2827, 2016.

Zhao, B., Wang, S. X., Liu, H., Xu, J. Y., Fu, K., Klimont, Z., Hao, J. M., He, K. B., Cofala, J., and Amann, M.: NOx emissions in China: historical trends and future perspectives, Atmos. Chem. Phys., 13, 9869-9897, doi:10.5194/acp-13-9869-2013, 2013.

Ziemke, J. R., A.R. Douglass, L.D. Oman, S.E. Strahan, and B.N. Duncan: Tropospheric ozone variability in the tropics from ENSO to MJO and shorter timescales, Atmos. Chem. Phys., 15, 8037–8049, 2015.